Low-frequency ac electrical resistivity of liquid gallium and its relationship with the dynamic structure factor

F. J. Bermejo,[1] L. Férnandez-Barquín,[2] J. García Soldevilla,[2] D. Gómez Plaza,[2] and J. C. Gómez-Sal[2]

[1] *Instituto de Estructura de la Materia, Consejo Superior de Investigaciones Científicas, Serrano 123, E-28006 Madrid, Spain*

[2] *Departamento de Ciencia e Ingeniería de la Tierra, el Terreno y los Materiales, Universidad de Cantabria, Avenida los Castros s/n, E-39005, Santander, Spain*

(Received 30 March 1994)

The low-frequency electrical resistivity of both liquid and solid gallium has been measured at several temperatures about the melting transition ($T_m = 302.8$ K), for frequencies comprised between 80 Hz and 100 kHz. The results regarding the frequency dependence of this quantity in the liquid phase are rationalized in terms of the hydrodynamic limit of the dynamic structure factors which has been recently discussed with the help of an effective potential derived from direct inversion of the experimental $S(Q)$ static structure factor. Finally the relevance of the present results regarding recent efforts directed towards the understanding of electronic transport properties of nonsimple liquid metals is briefly discussed.

PACS number(s): 62.10.+s, 72.15.Cz

I. INTRODUCTION

The understanding of the relationships between the ac electronic transport properties and the ionic dynamics encompassed in the $S(Q,\omega)$ structure factors has been repeatedly stated as one of the main aims of the theory of liquid metals [1, 2]. However, quantitative comparisons between the predictions brought forward by different theoretical approaches and experimental data are scarce, mainly as a consequence of the experimental difficulties encountered by measurements of both $S(Q,\omega)$ and the electronic frequency-dependent properties such as the $\rho(\omega)$ ac resistivity [or its inverse $\sigma(\omega)$] over comparable ranges of frequencies. As a matter of fact, experimental measurements of $\rho(\omega)$ seem to be bounded to frequencies below the MHz range (using the four-probe method), and above 10^{14} Hz (from optical-constant measurements), thus leaving unexplored the THz frequency range, where data regarding $S(Q,\omega)$ can be measured by neutron scattering or calculated from computer simulations.

The purpose of the present communication is thus to explore the predictive capability of some theoretical treatments by means of comparison of the calculated transport functions with experimental results, using data for liquid gallium as a case example. Such an endeavor constitutes a natural continuation of our previous work [3], where the dynamic structure factor as recently measured by neutron scattering was discussed with the aid of effective potentials derived from direct inversion of the $S(Q)$ structure factors [4]. A qualitative agreement between the experimental $S(Q,\omega)$ and the calculated ones reconstructed from the computed first two even-frequency moments [3] was found there (the calculated damping factors are well below the ones corresponding to the measured spectra) [3]. However, the fact that the effective potentials referred to are able to reproduce with acceptable accuracy most of the thermodynamics and elastic-constant data allows one to extrapolate the spectra well down into the hydrodynamic regime, using for the purpose the elastic and viscous properties derived from the previous study. In addition, as evidenced in the previous communication, acceptable values for the dc resistivity result from the calculations, something which lends further support to the extrapolation procedure adopted herein, since the zeroth-frequency limit of this property is recovered.

The interest in the study of the electronic transport processes in liquid gallium stems from the fact that, apart from its inherent technological importance, it constitutes an example of a polyvalent metal (along with Al, In, Si, Ge, Sn, Bi, etc.) which is normally regarded as "simple" as far as the electronic properties are concerned, showing, however, a substantial degree of intricacy regarding the atomic dynamics, or even its static properties [5]. Our aim is therefore to explore the extent to which the atomic dynamical effects affect the electronic properties, and so to verify its "simple liquid metal" character.

II. EXPERIMENTAL RESULTS

The experimental measurements were carried employing an ac four-probe method, using nickel-coated brass tips to make the electrical contacts. A sine wave signal was generated by a Hewlett Packard 3325A function generator, and the voltage was measured using a digital two-phase lock-in amplifier (Stanford Research SR 850 DSP) operated in the differential mode. The electric current passing through the circuit was calibrated by measuring the drop in current voltage in a 50 Ω resistance in series with the sample. Extreme precautions had to be taken in order to minimize the presence, at

high frequencies, of induced, parasitic currents. For such a purpose several shielding schemes were employed until these currents were reduced down to negligible levels. The temperature was regulated by means of an electrical resistance and monitored with an E-type thermocouple; the absolute accuracy in temperature measurements was estimated to be ≈ 0.5 K, and the estimate of the relative error in the measured resistivity was $\approx 0.1\%$. The sample was 99.9% pure gallium metal and was used without further purification. The sample holder was made of a polyvinyl chloride (PVC) block and the sample dimensions were $20 \times 2 \times 2.5$ mm^3. The absolute accuracy of the experimental measurements is strongly dependent upon the precise knowledge of the sample dimensions. The latter were difficult to measure with high accuracy since a rough metal surface is formed after rapid crystallization is induced by using the sharp point of a gallium crystal as a seed. In order to provide an absolute scale, use was made of the dc measurements of Ginter *et al.* [6], which report static data from 323.15 K up to ≈ 1370 K, showing an excellent linear temperature dependence. The data were then normalized using such a scale by calculating the normalization factor corresponding to the zeroth-frequency (dc) limit of our measurements.

The measured frequency dependence of $\rho(\omega, T)$ for the solid at 291.2 K and liquid at 321.2 K is shown in Fig. 1(a). The deceptively simple (i.e., quasilinear) behavior of the resistivity above 10 kHz is best unveiled from a plot of the conductivity $\sigma(\omega, T) = \rho^{-1}(\omega, T)$, as shown in Fig 1(b). As can be seen, the conductivities in both solid and liquid phases can roughly be described in terms of a Lorentzian function of widths 1.85×10^4 Hz for the solid and 2.36×10^4 Hz for the melt, plus a small ($\approx 6\%$) frequency-independent background. Such a description has, however, to be regarded as approximate since the systematic deviations from such idealized behavior (i.e., exponential decay of the fluctuations in current density) indicate that additional transport processes are operative. A time scale for the fluctuations being sampled can be set from the inverse of the widths of the fitted Lorentzians, giving values of 8.5×10^{-5} s for the solid and 6.8×10^{-6} s for the liquid. Such dependence on frequency thus evidences the dominance of extended states as far as electron conduction is concerned, the contributions arising from some other plausible conduction channels (i.e., hopping transport, tunneling, etc.) being hidden within the apparently frequency-independent background.

The measurements of the change in resistivity at the freezing transition were carried out following thermal cycles from room temperature up to 323 K which took a half hour, and then cooling down to 293 K during 2 h. The data were measured in a dynamic way, taking about 1 min per frequency. Crystallization was induced within the supercooled liquid using the seed described above, and the absence of any measurable difference in resistivity for all crystallizations indicates that the solid formed in such a way can be regarded as a polycrystal. If this were not the case, extreme variations in the resistivity after different freezing cycles would have been revealed [6]. Fig. 1(c) exemplifies the strong hysteresis effects revealed by the heating and cooling steps. The origin of such effects has to be ascribed to the well known tendency of the liquid to form a supercooled metastable phase. On the other hand, the comparison of resistivities for the solid and supercooled liquid at temperatures about 300 K serves to quantitatively differentiate the effects caused by the lack of long range order (after melting) from those due to temperature only.

Within the liquid phase, the resistivity shows a smooth temperature dependence which can be approximated by a straight line, yielding temperature coefficients $\alpha(\omega, T) = 1/\rho(\omega, T)\partial\rho(\omega, T)/\partial T$ of 9.89×10^{-4} K^{-1} at 80 Hz and 8.75×10^{-4} K^{-1} for 5 kHz at the melting point. The present data can be compared with the dc value given by Powell [6] of 7.54×10^{-4} K^{-1}, as well as with those of Ginter *et al.* [6], the observed differences being explainable in terms of the slight frequency dependence even at 80 Hz, as well as the differences in sample purity.

The ratio of the resistivity of the liquid at melting to that of the solid gives figures of 1.26 and 1.21 for the two frequencies mentioned, which are below those for molten

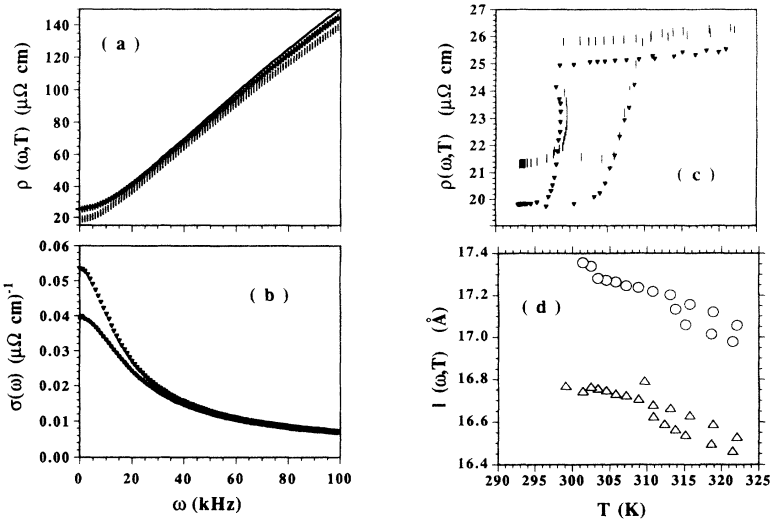

FIG. 1. (a) Frequency dependence of the ac resistivity. Data pertaining to the liquid phase are shown by crosses and the vertical bars show the data corresponding to the solid. The solid line shows the approximation to the data for the liquid calculated using Eq. (4). (b) Same data as in (a) plotted as electrical conductivities for liquid (filled dots) and solid (open triangles) Ga. (c) Temperature dependence of the measured resistivities, about the freezing transition. Filled inverted triangles correspond to measurements carried out at a frequency of 80 Hz, and the vertical bars stand for measurements at 5 kHz. (d) Temperature dependence of the electron mean free paths in the liquid phase. Circles correspond to measurements at 80 Hz and triangles to 5 kHz.

alkali metals (1.59 for Li or 1.69 for Cs) but well above those characteristic of strong scattering liquids such as Bi (≈ 0.40) or Te (≈ 0.07).

An idea of the electron scattering regime dominant in the liquid can be obtained from the electronic mean free paths calculated from $l(\omega,T) = v_F(T)\tau_\rho(\omega,T)$, where $v_F(T)$ stands for the temperature-dependent Fermi velocity (estimated from the density of valence electrons [7]) and the relaxation time was calculated from the measured resistivity at low (80 Hz) and high (5 kHz) frequencies. As can be seen from Fig. 1(d), the electron paths follow a quasilinear behavior with temperature, showing a mere $\approx 4\%$ decrease in the explored temperature range. The values of $l(\omega,T)$ indicate that in the dc limit paths of about seven times the distance to nearest neighbors, or about four times the Fermi wavelength, exist in the liquid, which can thus be characterized as an intermediate case between nearly-free-electron (NFE) metals (such as the alkali metals) and strong electron scatterers (such as molten transition metals or rare-earth elements), although it seems obviously closer to the former. In consequence, recourse to some of the theoretical approaches applicable to nearly-free-electron systems seems entirely justified.

As expected, the main effect of increasing the frequency translates into a concomitant reduction in the free paths, as also occurs with the temperature dependence. Also notice that a reduction of only $\approx 23\%$ in the free path takes place upon melting the solid, something which evidences the importance of electron scattering mechanisms taking place in the ordered phase at high temperatures. It is also worth noticing the fact that the free paths in the liquid at such high temperature are quite comparable to those reported for an amorphous Ga film by Hunderi and Ryberg [8] where estimates of 10–20 Åwere derived for this magnitude at T=10 K. An estimate of the free path of the liquid, assuming that the linear behavior holds down to 10 K, yields a value of 19.8 Å, a figure well within the limits quoted for the amorphous solid, which obviously suggests that the reduction in free-paths upon melting is mostly caused by static structural disorder, as will be discussed below.

III. DISCUSSION

As a first step in our analysis we have set out to carry out an evaluation of already existing (high-frequency) data [8], in order to assess to what extent deviations from the simple Drude-Zener behavior can unveil possible effects due to the blurring of the Fermi surface, something which could be expected to occur in this highly dense trivalent liquid. For such a purpose, use was made of the relationship [9]

$$\epsilon_1(\omega) - 1 = f(\omega) + 4\pi\tau\sigma_1(\omega) \ , \tag{1}$$

$$f(\omega) = \frac{\tau^2}{1+\omega^2\tau^2} h(\tau, n_e, T) \ , \tag{2}$$

which links the real part of the hydrodynamic limit of the complex dielectric function $\epsilon_1(\omega)$ to the real part of the conductivity $\sigma_1(\omega)$, in terms of a high-frequency relaxation time τ and a function $f(\omega)$ which accounts for the blurring of the Fermi surface through $h(\tau, n_e, T)$, where n_e stands for the density of valence electrons. A plot of $2n(\omega)k(\omega)\omega \propto \sigma_1(\omega)$ versus $1-\epsilon_1(\omega) = 1-n^2(\omega)+k^2(\omega)$, where $n(\omega)$ and $k(\omega)$ stand for the index of refraction and the propagation constant, should give a straight line passing through the origin with a slope $4\pi\tau$ if the NFE regime is obeyed, thus indicating that blurring effects accounted for by $f(\omega)$ are small or negligible. As shown in Fig. 2(a), and contrary to the case of liquid Na [10] where two different regimes are identifiable, the experimental points which correspond to two different sets [8] do not depart strongly from simple Drude behavior since the small finite value of the intercept depends noticeably on the chosen data set, and both of them constitute

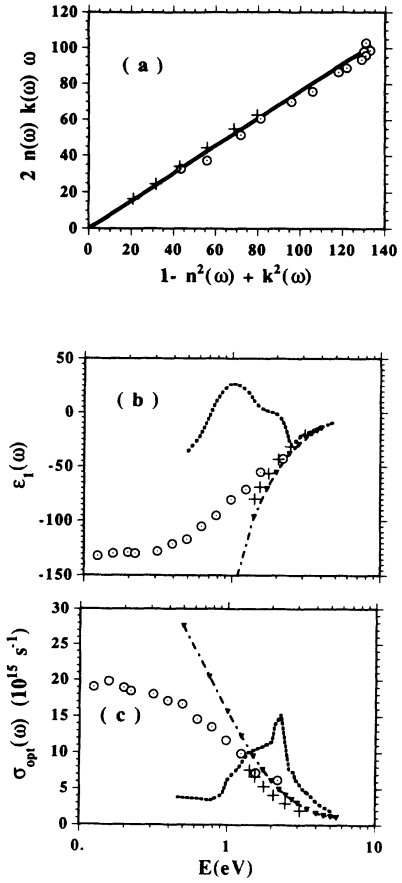

FIG. 2. (a) A plot showing $\epsilon_2\omega = 2nk\omega$ versus $1-\epsilon_1(\omega) = 1 - n^2 + k^2$ [see Eq. (1)]. The open symbols are quantities calculated from optical constants given by Comins in Ref. [8], the crosses correspond to those of Schulz [8], and the straight line gives the ideal (Drude) behavior with a relaxation time of 1.36×10^{-15} s calculated from the electronic density and the experimental resistivity at 321.2 K. (b) A comparison of the real part of the dielectric function for crystalline solid (dotted line, see Hunderi and Ryberg [8]), and amorphous Ga [8] (dash-dotted line with inverted triangles). Data for molten Ga are due to Comins [8] (circles with a dot), and Schulz [8] (crosses). (c) Optical conductivities for crystalline and amorphous solid Ga, and liquid. Same symbols as above are used.

acceptable realizations of NFE behavior. As a consequence, it seems clear that the effects of Fermi surface blurring have to be rather small, something which can also be ascertained from the estimated free paths, since the blurring ΔQ times the free paths can be interpreted as an uncertainty product which should be of the order of unity.

It is also instructive to compare the optical data for the liquid, a hot solid (a film obtained by deposition and annealed at 300 K [8]), and an amorphous film (see the papers by Hunderi and Ryberg in Ref. [8]) in order to assess whether any residual band structure still survives upon melting, and also to set a high-frequency reference to which the present resistivity data can be referred. Furthermore, the comparison between crystal, amorphous, and liquid data sets can also serve to separate those effects brought about by the lack of periodicity (quenched disorder) from those originated by the lack of true equilibrium positions for the ions (dynamical disorder in the liquid). Figures 2(b) and 2(c) depict the behavior at optical frequencies of $\epsilon_1(\omega)$ and the optical conductivity $\sigma_{\rm opt}(\omega) = \omega\epsilon_2(\omega)/4\pi$ for crystalline and amorphous solid and liquid phases [8]. The functions for the liquid exhibit a remarkable NFE behavior in both $\sigma_{\rm opt}(\omega)$ and $\epsilon_1(\omega)$, whereas strong features associated with an interband transition at 2.30 eV and a broad shoulder at about 1.3 eV characteristic of the absorption between parallel bands (see the papers by Hunderi and Ryberg in Ref. [8]) are clearly visible for the crystal. Of particular interest is the fact that the amorphous solid follows a rather close pattern to that of the liquid for energies above $\approx$ 1 eV, deviating from it at lower frequencies. Notice, however, that the optical spectra of both liquid and solid Ga start to be remarkably similar for frequencies above 3 eV. An estimate of the electron effective mass in the optical range $m^*_{\rm opt}$ for the liquid was also derived from such data since the dispersive part of the dielectric function can be expressed as a function of wavelengths as

$$\epsilon_1(\lambda) = (1 + 4\pi n_e\alpha + \epsilon_{1i}) - n_e e^2\lambda^2/m^*_{\rm opt}\pi c^2 \ , \qquad (3)$$

where the term inside the parentheses comprises contributions from the polarizability of ionic cores given in terms of a material constant $\alpha = 8.12 \times 10^{-30}$ m^{-3}, and a term accounting for interband absorption ϵ_{1i} which can be assumed to have a constant value at very low frequencies [11]. The estimate of $m^*_{\rm opt}$ from a linear plot of $\epsilon_1(\lambda)$ versus λ^2 gave a value of 1.009 times the electron mass, which is close to those estimated for molten light alkali metals (0.99 for Na and 0.97 for K [12, 2]), but above the calculated value of 0.96 given in ref. [12] for liquid gallium.

A first attempt for the analysis of the frequency dependence of the resistivity was carried out using the relationship for the long-wavelength limit of the longitudinal conductivity [13]

$$\sigma_L(\omega,T) = \frac{n_e(T)e^2}{m_e}\frac{M/m_i}{-i\omega + M\gamma(\omega,T)/n_e(T),m_i m_e} \ , \qquad (4)$$

where n_e stands for the (temperature-dependent) valence electron density, m_e is the electron mass, $M = m_i + Zm_e$, m_i being the ion mass and Z its valence, and the quantity $\gamma(\omega,T)$ represents a Fourier transform of the electronic force-force autocorrelation function. From the frequency-dependent resistivity, values for such a function were calculated once the resistivity relaxation time $\tau_\rho(\omega,T)$ was derived from $\tau_\rho(\omega,T) = m_e/\rho(\omega,T)n_e(T)e^2$, since $\gamma(\omega,T) = n_e(T)m_e/\tau_\rho(\omega,T)$. A comparison of the calculated values of $\mathrm{Re}(\sigma_L^{-1}(\omega,T))$ with the present measurement reveals that such an approximation can be considered as rather accurate [as long as all the frequency dependence is given by the experimentally derived values for $\gamma(\omega,T)$) for the polycrystalline solid (the differences between calculated and measured values are well within the experimental error). However, a systematic deviation between experimental and calculated quantities is found for the liquid, where, as shown in Fig. 1(a), the calculated function deviates from the measurement, the calculated curve lying above the experimental values. Such deviations become more important as the frequency is increased, and as a matter of fact, they exhibit the same frequency dependence as the experimental resistivity. Such a finding evidences the presence, within the liquid phase, of transport mechanisms not accounted for by Eq. (4). Since, as described above, the measured resistivity shows that the conduction regime still is far from the strong scattering case (i.e., free paths comparable to the Fermi wavelength), the observed discrepancy should be better ascribed to some simplifying assumptions built in to the derivation of Eq. (4), rather than to the appearance after melting of some random tunneling processes of the kind postulated to explain the dc conductivity of strong scattering materials [14].

In the following we will focus our attention on the relationships between the measured resistivity (or conductivity) and the dynamic structure factor relevant for electronic transport processes, that is, $S_{ii}(Q,\omega)$ (i.e., the ionic dynamic structure factor). For such a purpose recourse was made to the expression originally developed by Hinkelman [15] for the hydrodynamic (i.e., $\lim Q \longrightarrow 0$) limit of the external conductivity $\sigma^e(\omega,T)$:

$$\mathrm{Re}\sigma^e(\omega,T) = \frac{\pi e^2 M^2\omega}{m_e^2}[1 - \exp(-\hbar\omega\beta)] \lim_{Q\to 0}\frac{S_{ii}(Q,\omega,T)}{Q^2} - \frac{\pi n_i M e^2}{m_e^2}\delta(\omega) \qquad (5)$$

$$= \frac{\sigma_1(\omega,T)}{\epsilon_1^2(\omega) + \left(\frac{4\pi\sigma_1(\omega,T)}{\omega}\right)^2} \ , \qquad (6)$$

where the real part of $\sigma^e(\omega,T)$ is written in terms of the real part of the conductivity $\sigma_1(\omega,T)$ and the long-wavelength limit of the dielectric function $\epsilon_1(\omega)$ (assumed to be independent of temperature because of the lack of experimental data as well as the rather smooth dependence on frequency within the region of interest). $S_{ii}(Q,\omega,T)$ is the dynamic structure factor for the ions, $\beta = 1/k_B T$ and the rest of the symbols have already been defined. Following March and Paranjape [16], the equation written above can be recast as

$$\frac{16\pi^2}{\omega^2}\sigma_1^2(\omega,T) - g(\omega,T)\tilde{S}(\omega,T)\sigma_1(\omega,T) + \epsilon_1^2(\omega) = 0 \ , \tag{7}$$

where $g(\omega,T)$ is the inverse of the factor multiplying the limit in Eq. (5), and $\tilde{S}(\omega,T) = [\lim_{Q\to 0} S_{ii}(Q,\omega,T)/Q^2]^{-1}$, from which estimates of $\tilde{S}(\omega,T)^{-1}$ can be derived from the measured values of the frequency-dependent conductivity if the behavior of $\epsilon_1(\omega)$ in the required range of frequencies is known. Since accurate experimental data regarding the latter quantity seem to be extremely difficult to measure at low frequencies, estimates of it were derived from extrapolation of data shown in Fig. 2(b) which were approximated by a broad inverted Lorentzian (see the paper by Comins in Ref. [8]). Solution of the above equation thus gives the long-wavelength limit of the ionic structure factor and the frequency dependence of such a quantity is shown in Fig. 3. As can be seen, the calculated spectrum shows a steep dependence on the frequency, without evidencing any low-frequency feature, and further comments are deferred to the next paragraph. A similar procedure could not be followed for the solid because of the lack of optical data for energies below 0.5 eV, as well as the difficulty of extrapolating to zero frequency the steep curve shown in Fig. 2(b).

Alternatively, $\tilde{S}(\omega,T)^{-1}$ can be calculated from hydrodynamic models for the relevant quantities entering the structure factor. Such a calculation requires the specification of $S_{ii}(Q,\omega,T)$ which should contain the contribution of the ionic motions to the plasmon spectrum and therefore cannot be equated to the structure factor measured by neutron scattering after an extrapolation to the hydrodynamic limit is made. However, closed-form expressions for $S_{ii}(Q,\omega,T)$ have been derived by Tosi *et al.* [15], which enable one to write this quantity as a sum of atomic and plasma contributions. The former can be identified with the one accessible by experimental means if proper account is made of thermal conduction effects, a point disregarded in the original formulation since the derivation was made assuming that the ratio of specific heats $\gamma = C_p/C_v = 1$. Upon consideration of such effects, a somewhat more generalized expression for the dynamic structure factor reads

$$S_{ii}(Q,\omega,T) = \frac{\omega\beta}{[1-\exp(\hbar\omega\beta)]}\frac{Q^2}{\pi M}\left[S(Q)\left\{\left(1-\frac{1}{\gamma}\right)\frac{D(T)}{\omega^2+[D(T)Q^2]^2} + \frac{1}{2\gamma\omega_0(Q)}\frac{4\omega\omega_0(Q)\Gamma(Q)}{[\omega^2-\omega_0^2(Q)]^2+4\omega^2\Gamma^2(Q)}\right\}\right.$$
$$\left. + v_0(T)\frac{M^2\gamma(\omega,T)/m_i^2}{(\omega^2-\omega_p^2)^2+[M\omega\gamma(\omega,T)/n_e m_i m_e]^2}\right], \tag{8}$$

where the first term specifies the detailed balance condition, the first one within the large square brackets accounts for nonpropagative thermal (entropy) fluctuations given in terms of the coefficient of thermal diffusivity $D(T)$, the second comprises sound-mode contributions characterized by a frequency $\omega_0(Q) = cQ$ and a damping term $\Gamma(Q) = \frac{1}{2}[D(T)(\gamma-1) + \frac{4}{3}\eta_s(Q) + \eta_b]$ specified by the shear η_s and bulk η_b coefficients of viscosity, and the third gives the contribution of the ions to the plasmon peak, which is characterized by a plasma frequency ω_p, a damping term dependent on the Fourier transform of the force autocorrelations $\gamma(\omega,T)$ which was considered in the above paragraphs, and $v_0(T)$, the thermal velocity of the ions. From knowledge of the experimental values of the thermal conductivity of the liquid [7] as well as its specific heat [7], the values of $D(T)$ are found to be 1.17×10^{-6} m^2 s^{-1} at the melting point, which results in noticeable linewidths for the Rayleigh peak even at the low-Q values characteristic of this kind of experiment $Q \approx 10^{-8}$ Å^{-1}. As far as the sound-mode contributions are concerned, explicit information regarding the frequencies and damping terms can be obtained from our previous work [3]. The modeling of the plasmon term requires a knowledge of the $\gamma(\omega,T)$ function, a topic discussed above, as well as the plasma frequency, which for our purposes can be identified with that for the free electrons, and gives values of about 3.56×10^{15} Hz at the melting point (the reported values for the liquid and amorphous film are 3.58×10^{15} Hz and 3.46×10^{15} Hz, respectively; see the papers by Hunderi and Ryberg in Ref. [8]). The relative weight of the plasmon part with respect to entropy and density fluctuations could be expected to be small from consideration of the mass factors entering the equation as well as from the large value of ω_p.

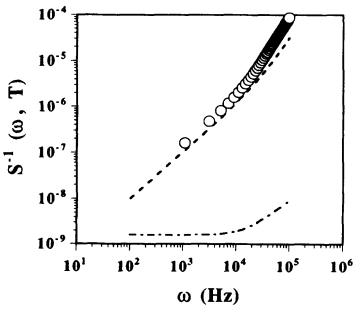

FIG. 3. Experimental estimate of $\tilde{S}(\omega,T)^{-1}$ (open circles) and contributions calculated using Eq. (8). The collective mode spectrum is shown as dashes and the plasmon contribution by a dash-dotted line.

A comparison between the calculated and experimental estimates of $\tilde{S}(\omega,T)^{-1}$ is provided in Fig. 3. As can be seen, the spectral shape of the calculated function

would turn out to be comparable to that derived from experiment if the contribution from the Rayleigh wing is omitted, although the experimental curve shows a far more steep behavior. Consideration of the three different contributions entering Eq. (8), shows that arising from the plasmon part is far too small, due to the large value of the plasma frequency, to account for the observed intensity. Most of the intensity should then arise from the sound-mode contributions to the structure factor, and, as shown in the graph, the intensity arising from the tail of a hydrodynamic phonon band with $Q \approx 3.5 \times 10{-}8$ Å^{-1}, and a propagation frequency corresponding to that given in Ref. [3], can account, in part, for such extra intensity.

In consequence, it seems clear that, although Eq. (4) can give a semiquantitative account of the measured resistivity in the liquid, it does so because the frequency dependence of $\gamma(\omega, T)$, which is derived from experiment, is used as input data. Far poorer results are obtained if such a function is calculated assuming a simple exponential decay of the current fluctuations, as explained in the previous section. Therefore the result given by Eq. (4) would be better tested if values for the frequency dependence of $\gamma(\omega, T)$ are derived from other means.

In order to shed more light onto the resistive mechanisms operating at such low frequencies, consideration was made of the long-wavelength low-frequency limits of the dynamic structure factor, which gives for the experimental resistivity [13, 17]

$$\rho(T) = \pi\beta \left(\frac{4\pi e M}{m_e}\right)^2 \lim_{\omega\to 0} \lim_{Q\to 0} \left[\frac{S_{ii}(Q,\omega)}{Q^2}\right]. \qquad (9)$$

Using the temperature dependence of the dc values given by Ginter *et al.* [6], the behavior with temperature of $\lim_{\omega\to 0} \lim_{Q\to 0} \left[\frac{S_{ii}(Q,\omega)}{Q^2}\right]$ was calculated and the result is shown in Fig. 4(a). To investigate the origin of such a dependence in terms of the contributions entering the structure factor, the behavior with temperature of several dynamical quantities was analyzed. An obvious starting point, therefore, was to analyze the temperature dependence of $\gamma(T)$ as derived from the dc values of the resistivity relaxation time through $\gamma(T) = \tau_\rho^{-1} n_e(T) m_e$, and the result is shown in Fig. 4(b). Comparison of the curvature of the graphs displayed in Figs. 4(a) and 4(b) thus evidences a rather disparate behavior indicating that some other mechanisms should be sought to explain the temperature dependence shown in Fig. 4(a). The linear dependence of the resistivity on temperature in both liquid and solid phases suggests that most of the electronic scattering processes are due to thermal vibrations. In such a respect, it is worth remarking that the figure of merit regarding such a contribution is nothing less than the total atomic mean-square displacement $\langle u^2(T)\rangle$ since $\rho(T) \propto \tau_\rho^{-1} \propto \langle u^2(T)\rangle$, and that for a liquid should contain contributions arising from zero-frequency (diffusive) motions $\langle u^2_{\mathbf{self}}(T)\rangle$ as well as from others originating from collective, higher frequency modes. A separation of both contributions becomes difficult unless detailed information regarding the former is available from experiment or simulational means [18]. A simple estimate of such a contribution was nonetheless attempted from a Debye relationship $\langle u^2_{coll}(T)\rangle \propto \hbar^2 Q_D^2 k_B T / M(k_B\Theta)^2$ using for the purpose the value of the Debye temperature $\Theta_D = 240$ K and cutoff $Q_D = 1.16$ Å^{-1} for the solid, which obviously results in a contribution linear in T. An estimate

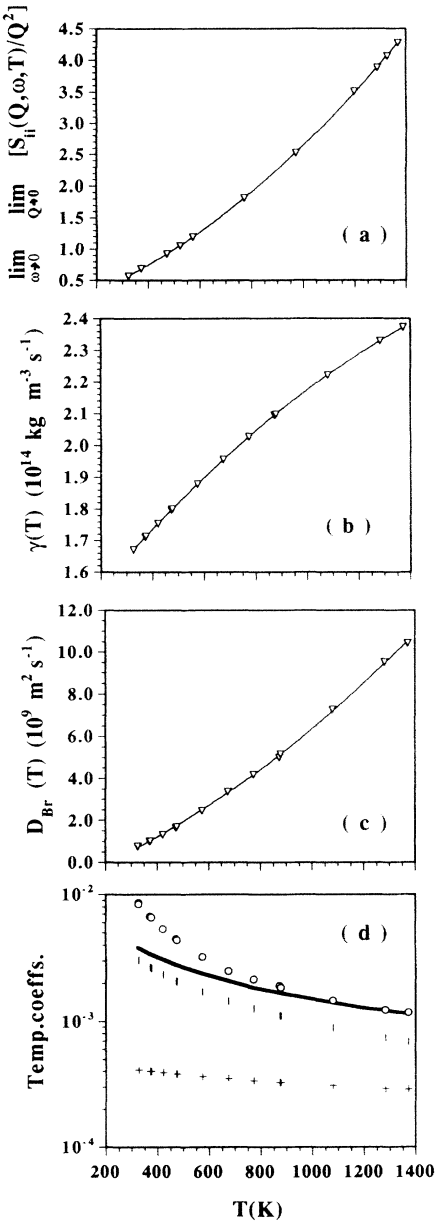

FIG. 4. (a) Temperature dependence of the hydrodynamic, zero-frequency limit of the dynamic structure factor [see Eq. (9)]. (b) Temperature dependence of $\gamma(T)$ derived from dc values of the resistivity and accounting for the temperature dependence of the valence electron density. (c) Temperature dependence of the self-diffusion coefficient as calculated from the experimental values of the shear viscosity by means of a Stokes-Einstein relationship. The solid line in the graph represents a second degree polynomial approximation to the data. (d) Temperature coefficients for the ionic dynamic structure factor (solid line), diffusion coefficient (open circles), contributions from collective motions (vertical bars), and $\gamma(T)$ (crosses).

of the total mean-square displacement for a liquid can nonetheless be derived from the self-diffusion coefficient. Estimates for such a magnitude were then derived from the experimental values for the shear viscosity by means of a brownian approximation, $D_{\mathrm{Br}}(T) = k_B T/4\pi\eta_s R_a$, where $R_a = 2.6$ Å, the particle radius. The temperature dependence of the self-diffusion coefficient is then plotted in Fig. 4(c), where it can be seen that such a dependence comes rather close to that exhibited by the limiting values of the structure factor, specially at temperatures well above melting. To compare the temperature dependence of the different magnitudes on a common scale, Fig. 4(d) displays their temperature coefficients defined through $TC(x) = (1/x)\partial x/\partial T$. As can be seen, the values of such a coefficient regarding the ionic dynamic structure factor, lie at temperatures below 800 K between those referred to the total atomic displacement and those for $\langle u^2_{\mathrm{coll}}\rangle$, whereas at higher temperatures the coefficient associated with the dynamic structure factor closely follows that for the total displacement. Such a finding can be tentatively interpreted as a crossover between two mechanisms causing resistance to electronic conduction, which goes from a low temperature regime (below about 400–600 K) where higher frequency motions are more effective in reducing the electronic free paths, to one where the resistance seems to be dominated by fully incoherent motions.

Finally, it is worth considering some plausible explanations regarding the absence of well defined (i.e., underdamped) excitations in the $S(Q,\omega)$ dynamic structure factor measured by neutron scattering which was analyzed in our previous communication [3]. As mentioned there, from the macroscopic properties of this liquid (i.e., ratio of specific heats and shear viscosity) it could be expected that propagating short-wavelength excitations would reveal themselves in the neutron experiment at wave numbers ≈ 1 Å^{-1} and frequencies in the THz range. From the analysis of the wave-vector dependence of the longitudinal viscosity [i.e., $\eta_l(Q) = 4/3\eta_s(Q) + \eta_b$], it was inferred [3] that a rather large value of the η_b bulk viscosity coefficient (plus perhaps a thermal conduction term [20]) was the main contribution to the damping of the excitations. The microscopic origin of such a bulk viscosity term is difficult to ascertain. However, some insight may be gained if the analysis of the extra damping (bulk viscosity) is couched in terms of the absorption due to the viscosity of valence electrons. Following well established treatments based on the Boltzmann transport equation for the homogeneous electron gas [19], the attenuation of longitudinal sound waves by interactions with the electron gas is given as attenuation per wavelength as

$$\alpha(\lambda) = \frac{8\pi^2}{15}\frac{m_e n_e v_F^2}{m_i n_i v_s^2}\omega\tau \ , \tag{10}$$

where v_F stands for the Fermi velocity, v_s for the adiabatic speed of sound, and values for the relaxation time τ are estimated from the dc values of the resistivity. Such a formula, which is valid for long wavelengths [i.e., $Ql(\omega,T) \ll 1$], predicts a linear dependence of the attenuation on frequency, and approaches in the opposite $Ql(\omega,T) \gg 1$ limit a frequency-independent regime. It is then instructive to compare the present case with that of liquid Rb [20], a liquid with macroscopic properties not too dissimilar from Ga, where the presence of finite-frequency excitations has been confirmed by neutron and computer simulation means. Substitution of the numerical values for Ga and Rb in the formula given above yields, for frequencies of 1 THz, attenuation factors of 0.65 and 0.17, respectively; sound waves in liquid Ga are attenuated about 3.8 times more than in Rb due to the electronic viscosity term, a figure which comes close to the ratio of longitudinal to shear viscosities (4.2) estimated in our previous communication. As a consequence of such an analysis, it could then be possible to estimate a relaxation time $\tau_2 = \eta_e/\frac{1}{5}n_e m_e v_F^2$ associated with the viscosity of the electron gas η_e [21], if the order of magnitude of the latter is equated to that of η_b. The result of such an exercise upon substitution of the relevant constants yields $\tau_2 \approx 10^{-14}$ s, which is substantially higher than the resistivity relaxation time $\tau_\rho = 8.78 \times 10^{-16}$ s, and comes close to the upper edge of the vibrational frequency distribution ($\approx 6 \times 10^{13}$ s^{-1}).

IV. CONCLUSIONS

The present communication shows that, contrary to what may be expected from the relatively complex liquid structure of molten gallium, its electronic transport processes can be well taken account of in terms of a simple NFE model. Such a finding goes along with the calculations of Hafner and Jank [22], and with photoemission experiments due to Greuter *et al.* [23] on the electronic density of states (DOS) of molten and solid Ga, which evidence that after melting a nearly complete NFE behavior is approached. As a matter of fact, the structured DOS seen in the solid, exhibiting a dip at the Fermi level indicative of partial covalency effects, is completely removed after melting, where only a very shallow feature at 3 eV below the Fermi energy is seen, and the DOS can be well described in terms of a parabolic NFE model.

The low-frequency ac resistivity of this liquid metal can be understood in, at most, semiquantitative terms from a model for the ionic dynamic structure factor calculated from tabulated values of the relevant transport magnitudes, provided that the low frequency dynamics associated with entropy fluctuations is disregarded.

A consideration of the mean free paths of both crystalline and amorphous solids and the liquid clearly suggests that the decrease in electron paths after melting is mainly caused by the appearance of static disorder, the effects of thermal motions being mainly reflected by the temperature dependence of the measured resistivity. The relatively small increase in resistivity after melting can thus be rationalized in terms of two competing mechanisms. In fact, some effective electron scattering mechanisms present in the solid as revealed by the structured DOS [22], as well as the strong exciton and interband absorptions [see Figs. 2(a) and 2(b)], clearly disappear above T_m. An increased value of the DOS of electronic states at the Fermi level upon melting, as well as the presence of some additional mechanisms linked to the ionic

conduction (mass diffusion), thus seem to partially counterbalance the absence of any significant Bloch-Grüneisen contribution in the liquid.

The results reported in the present work also help to explain the absence of well defined short-wavelength finite-frequency excitations reported in our previous communication [3], since a comparison with the well established case of liquid Rb evidences the role of the electronic viscosity as a source of damping of longitudinal sound.

ACKNOWLEDGMENTS

This work has been supported in part by DGICYT, Grant No. PB92- 0114-C04.

[1] N.H. March, *Liquid Metals: Concepts and Theory*, Cambridge Monographs on Mathematical Physics (Cambridge University Press, Cambridge, England, 1990).

[2] T.E. Faber, *Theory of Liquid Metals* (Cambridge University Press, Cambridge, England, 1972).

[3] F.J. Bermejo, M. Garcia-Hernandez, J.L. Martinez, and B. Hennion, Phys. Rev. E **49**, 3133 (1994).

[4] M.C. Bellisent-Funel, P. Chieux, D. Levesque, and J.J. Weis, Phys. Rev. A **39**, 6310 (1989).

[5] X.G. Gong, G.L. Chiarotti, M. Parinello, and E. Tosatti, Europhys. Lett. **21**, 469 (1993); see Phys. Rev. B **43**, 14 277 (1991) for a similar calculation regarding α-Ga. Partial covalency effects have been repeatedly adduced as an explanation of the decrease in molar volume after melting (about 3% in Ga).

[6] R.W. Powell, Proc. R. Soc. London Ser. A **209**, 525 (1951). A more recent compilation of available data can be found in G. Ginter, J.G. Gasser, and R. Kleim, Philos. Mag. B **54**, 543 (1986).

[7] The density, adiabatic sound velocity, and sound attenuation are taken from M. Inui, S. Takeda, and T. Uechi, J. Phys. Soc. Jpn. **61**, 3203 (1992). The values for the viscosity and specific heat have been taken from the *CRC Handbook of Chemistry and Physics*, 74th ed. (Chemical Rubber, Boca Raton, 1993). Thermal conductivities were taken from M.J. Duggin, Phys. Lett. A **29**, 470 (1969).

[8] Optical constants for molten Ga were taken from L.G. Schulz, J. Opt. Soc. Am. **47**, 64 (1957); Adv. Phys. **6**, 102 (1957); N.R. Comins, Philos. Mag. B **25**, 817 (1972). Data for solid films of Ga at 300 K were taken from O. Hunderi and R. Ryberg, J. Phys. F **4**, 2084 (1974). The data regarding quenched Ga (amorphous) films at 10 K were taken from O. Hunderi and R. Ryberg, J. Phys. F **4**, 2096 (1974).

[9] In Ref. [1], Eq. 10.63, p. 142.

[10] T. Inagaki, E.T. Arakawa, R.D. Birkoff, and M.W. Williams, Phys. Rev. B **13**, 5610 (1976).

[11] Both α and ϵ_{1i} are assumed to be independent of the wavelength. More detailed calculations, such as those reported by K. Sturm, E. Zaremba, and K. Nuroh [Phys. Rev. B **42**, 6973 (1990)], which treat the interaction between the core dipoles and the valence electron gas in a self-consistent manner, evidence a logarithmic singularity at high frequencies (near the core threshold).

[12] In Ref. [2], Table 5.7, p. 387.

[13] In Ref. [1], p. 292.

[14] For a review of this topic see, for instance, W. van der Lugt and W. Geertsma, Can. J. Phys. **65**, 326 (1987). Explicit calculations of the importance of a random tunneling mechanism are given by D. Belitz and W. Schirmacher, J. Phys. C **16**, 913 (1983), and references therein. Calculations based on numerical computations over clusters of some few hundred atoms have been carried out among others by L.E. Ballentine and J.E. Hammerberg, Can. J. Phys. **62**, 692 (1984); S.K. Bose, O. Jepsen, and O.K. Andersen, Phys. Rev. B **48**, 4265 (1993).

[15] The expression was first derived by H. Hinkelman, Phys. Lett. **33A**, 479 (1970), and later reworked by M. Tosi, M. Parinello, and N.H. March, Nuovo Cimento B **23**, 135 (1974).

[16] N.H. March and B.V. Paranjape, Phys. Chem. Liquids **17**, 55 (1987).

[17] W. Jones, J. Phys. **3**, 1577 (1973).

[18] A computer molecular dynamics simulation using the effective potentials given in [4] was carried out for this purpose. The resulting diffusion coefficients were about half of those experimentally determined as reported in the literature, something which casts some doubt on the reliability of separating the two contributions by such a means even if empirical potentials of the kind considered here are available.

[19] A.B. Bathia, *Ultrasonic Absorption* (Dover, New York 1985), p. 302.

[20] The ratio of specific heats, shear viscosity, thermal conductivity, and dc resistivity for molten Rb are 1.15, 0.67 cP, 0.53 W cm^{-1} K^{-1}, and 22.5 $\mu\Omega$ cm, respectively, which come close to those of those of liquid Ga, although the heat conduction term of Rb is larger. Notice that the main difference between the macroscopic properties of these liquids regards the very different electronic number densities which amount to 0.1575 valence electrons $Å^{-1}$ for Ga at T=326 K and 0.0106 $Å^{-1}$ for Rb at T=316 K, and that damping effects due to heat diffusion are comparable in both liquids.

[21] H. Smith and H.H. Jensen, *Transport Phenomena* (Oxford University Press, Oxford, 1989), p. 114.

[22] J. Hafner and W. Jank, Phys. Rev. B **42**, 11 530 (1990).

[23] F. Greuter and P. Oelhafen, Z. Phys. B **34**, 123 (1979).